Chandra Observations of the Components of Clusters, Groups, and Galaxies and their Interactions*

W. Forman[1], C. Jones[1], M. Markevitch[1,3], A. Vikhlinin[1,3], and E. Churazov[2,3]

[1] Smithsonian Astrophysical Observatory, 60 Garden St. Cambridge, MA USA
[2] Max-Planck-Institut für Astrophysik, Karl-Schwarzschild-Strasse 1, 85741 Garching, Germany
[3] Space Research Institute (IKI), Profsoyuznaya 84/32, Moscow 117810, Russia

Abstract. We discuss two themes from Chandra observations of galaxies, groups, and clusters. First, we review the merging process as seen through the high angular resolution of Chandra. We present examples of sharp, edge-like surface brightness structures "cold fronts", the boundaries of the remaining cores of merger components and the Chandra observations of CL0657, the first clear example of a strong cluster merger shock. In addition to reviewing already published work, we present observations of the cold front around the elliptical galaxy NGC1404 which is infalling into the Fornax cluster and we discuss multiple "edges" in ZW3146. Second, we review the effects of relativistic, radio-emitting plasmas or "bubbles", inflated by active galactic nuclei, on the hot X-ray emitting gaseous atmospheres in galaxies and clusters. We review published work and also discuss the unusual X-ray structures surrounding the galaxies NGC4636 and NGC507.

1 Introduction

With its first images, the Einstein Observatory changed our view of clusters and galaxies. Clusters, rather than being dynamically old, relaxed systems showed extensive substructure reflecting complex gravitational potentials with "double" clusters merging on times scales of $\sim 10^9$ yrs [31,32,19]. Luminous elliptical galaxies, rather than being gas poor, were instead found to be gas rich systems with *hot* coronae having masses up to $\sim 10^9$ $M_\odot$ [21]. ROSAT and ASCA continued the revolution with studies of cluster merging and substructure including Coma, A2256, A754, Cygnus A, Centaurus, A1367,and Virgo, to mention just a few [4,5,1,51,29,30,28,52,7,37,10,46,35].

The high angular resolution provided by Chandra has again brought us new views of old friends – early type galaxies and clusters of galaxies – that we thought we knew pretty well. We are familiar with the ingredients, galaxies, radio emitting plasma, hot gas, and dark matter. The recipe is simple – *mix vigorously.* With these simple instructions we find new and unexpected phenomena in the Chandra observations.

* Contribution for the *Lighthouses of the Universe Conference*, 6-10 August 2001, Garching bei Munchen, Germany

2 A New Aspect of Cluster Mergers – Cold Fronts

For many years clusters were thought to be dynamically relaxed systems evolving slowly after an initial, short-lived episode of violent relaxation. However, in a prescient paper, Gunn & Gott argued that, while the dynamical timescale for the Coma cluster, the prototype of a relaxed cluster, was comfortably less than the Hubble time, other less dense clusters had dynamical timescales comparable to or longer than the age of the Universe [26]. Gunn & Gott concluded that "The present is the epoch of cluster formation". With the launch of the Einstein Observatory came the ability to "image" the gravitational potential around clusters. Many papers in the 1980's exploited the imaging capability of the Einstein Observatory and showed the rich and complex structure of galaxy clusters.

The X-ray observations supported the now prevalent idea that structure in the Universe has grown through gravitational amplification of small scale instabilities or hierarchical clustering. At one extreme, some clusters grow, in their final phase, through mergers of nearly equal mass components. Such mergers can be spectacular events involving kinetic energies as large as $\sim 10^{64}$ ergs, the most energetic events since the Big Bang. More common are smaller mergers and accretion of material from large scale filaments. An example showing the relationship between large scale structure and cluster merging is seen in the ROSAT image of A85 where small groups are detected, infalling along a filament into the main cluster. The central cluster galaxy, the bright cluster galaxies, an X-ray filament and nearby groups and clusters all show a common alignment at a position angle of about 160° extending from 100 kpc (the outer isophotes of the central cD galaxy) to 25 Mpc (the alignment of nearby clusters) [12]. Such common alignments over a wide range of scales are expected if clusters form through accretion of matter from filaments [49].

Chandra's high angular resolution has further illuminated the merging process and the complexity of the X-ray emitting intracluster medium (ICM). Prior to the launch of Chandra, sharp gas density discontinuities had been observed in the ROSAT images of A2142 and A3667 [37]. Since both clusters exhibited characteristics of major mergers, these features were expected to be shock fronts. However, the first Chandra observations showed that these were not shocks, but a new kind of structure – cold fronts [36]. Their study has provided new and detailed insights into the physics of the ICM [53,54].

2.1 Cold Fronts in Cluster Mergers

The first cold front observed by Chandra was in the hot ($kT \sim 9$ keV), X-ray-luminous cluster A2142 ($z = 0.089$). Two bright elliptical galaxies, whose velocities differ by 1840 km s^{-1} lie near the cluster center and are aligned in the general direction of the X-ray brightness elongation [36]. A2142 exhibits two sharp surface brightness edges – one lies $\sim 3'$ northwest of the cluster center (seen earlier in the ROSAT image) and a second lies $\sim 1'$ south of the center [36]. The gas temperature distributions across the edges show sharp and significant *increases* as the surface brightness (gas density) *decreases* [36]. The gas density

changes across the edges compensate, within the uncertainties, for the temperature increases so that the gas pressures across the edges are consistent with being equal. One possible origin of the A2142 structures is that they arise from the merger of two inter-penetrating systems whose dense cores have survived the merger process [36]. We observe A2142 as it would appear after the shock fronts have passed by each of the dense cores. The outer, lower density gas has been shock heated, but the dense cores remain "cold" [36]. Each sharp edge is then a boundary of a ram pressure-stripped subcluster core.

A particularly beautiful example of a cold front is seen in the Chandra observation of the Fornax cluster. In Fig. 1a, we see gas bound to the infalling bright elliptical galaxy NGC1404 as it approaches the cluster center (to the northwest). The image clearly shows the sharp edge of the surface brightness discontinuity, shaped by the ram pressure of the cluster gas. The temperature map (Fig. 1b) confirms that the infalling cloud is cold compared to the hotter Fornax ICM.

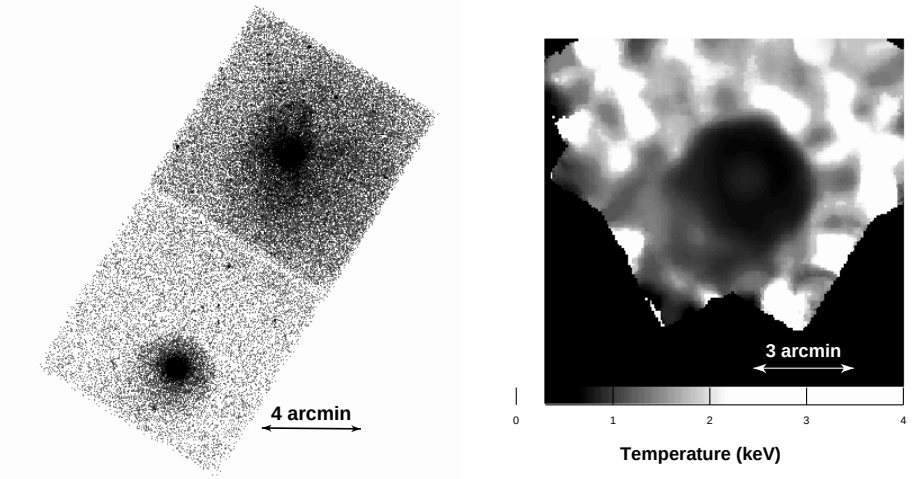

Fig. 1. The ACIS observation of NGC1404 and NGC1399. (**a**) shows the 0.5–2.0 keV band image of the Fornax cluster. The gas filled dark halo surrounding NGC1404 is at the lower left (southeast) while the cluster core, dominated by the halo surrounding NGC1399 lies at the upper right (northwest). (**b**) The temperature map of the Fornax region. The cold core surrounding NGC1404 has a temperature of less ~ 1 keV while the surrounding gas has a temperature of $\gtrsim 1.5$ keV.

Another example of a galaxy infalling into a cluster potential is M86. X-ray emission from M86 was first observed with the Einstein Observatory and subsequently by ROSAT. Its unusual "plume" was explained as a ram pressure stripped galactic corona produced as M86 crosses the core of the Virgo cluster at supersonic velocity [20,14,56,45]. The Chandra image and temperature map confirm a cool (~ 0.6 keV) corona embedded in the hot (~ 3 keV) Virgo ICM [22]. Based on the difference between the velocity of M86 and the Virgo cluster core,

about $\sim$1500 km sec^{-1}, M86 must be crossing the Virgo core at supersonic velocity. However, we see no clear cold front as in NGC1404 (for the image and temperature map of M86 see Fig. 6 and Fig. 7 in Forman et al. [22]). The most likely explanation is that M86 is moving nearly in the line of sight, directly towards us, and the resulting cold front (and possible shocks) are difficult to see in projection.

2.2 Cluster Physics and Edges

A3667, a moderately distant cluster ($z = 0.055$), also was expected to exhibit a shock front based on its ROSAT image [37]. However, as with A2142, the sharp feature is the boundary of a dense cold cloud, a merger remnant [53,54]. As Vikhlinin et al. showed, the edge is accurately modeled as a spheroid (see Fig. 2a) [53]. From the surface brightness profile, converted to gas density, and precise gas temperatures, the gas pressure on both sides of the cold front can be accurately calculated. The difference between the two pressures is a measure of the ram pressure of the ICM on the moving cold front. Hence, the precise measurement of the gas parameters yields the cloud velocity. The factor of two difference in pressures between the free streaming region and the region immediately inside the cold front yields a Mach number of the cloud of 1 ± 0.2 (1430 ± 290 km s^{-1}) [53].

In addition to the edge, a weak shock is detected. The distance between the cold front and the weak shock ($\sim$350 kpc) and the observed gas density jump at the shock (a factor of 1.1-1.2) yield the shock's propagation velocity, $\sim$1600 km s^{-1}, which is consistent with that derived independently from the pressure jump across the cold front [53].

The A3667 observation provides important information on the efficiency of transport processes in clusters. As the surface brightness profile shows (see Fig. 2), the density "edge" is very sharp. Quantitatively, Vikhlinin et al. found that the width of the front was less than $3.5''$ (5 kpc). This sharp edge requires that transport processes across the edge be suppressed, presumably by magnetic fields. Without such suppression, the edge should be broader since the relevant Coulomb mean free path for electrons is about 13 kpc, several times the width of the cold front [53]. Furthermore, Vikhlinin et al. observed that the cold front appears sharp only over a sector of about $\pm30^\circ$ centered on the direction of motion, while at larger angles, the sharp boundary disappears [54]. The disappearance can be explained by the onset of Kelvin-Helmholtz instabilities, as the ambient ICM gas flows past the moving cold front. To explain the observed extent of the sharp boundary, the instability must be partially suppressed, e.g., by a magnetic field parallel to the boundary with a strength of $7-16\mu$G. Such a parallel magnetic field may be drawn out by the flow along the front. This measured value of the magnetic field in the cold front implies that the pressure from magnetic fields is small (only 10-20% of the thermal pressure) and, hence, supports the accuracy of cluster gravitating mass estimates derived from X-ray measurements that assume that the X-ray emitting gas is in hydrostatic equilibrium and is supported by thermal pressure [54].

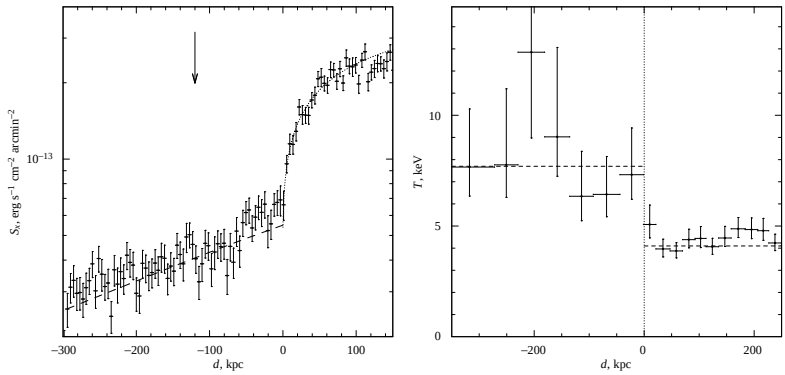

Fig. 2. (**a**) The surface brightness profile of A3667 extracted in elliptical regions across the cold front. The sharp "edge" is clearly seen. The dashed line is the ROSAT PSPC fit to the outer surface brightness distribution and agrees well with the Chandra observation. The dotted curve is a fit to a spheroid with a sharp boundary. The vertical arrow indicates the position of the weak shock. As discussed by Vikhlinin et al., the excess at distances of 0-50 kpc in front of the edge represents gas that accumulates in the stagnation region [53]. (**b**) The temperature profile across the cold front. The temperature *increases* from ~ 4 keV to ~ 8 keV across the front.

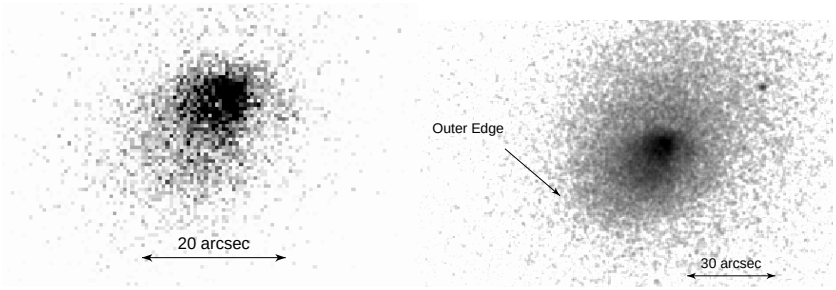

Fig. 3. Multiple X-ray surface brightness edges in ZW3146 ($z = 0.296$). (**a**) The 0.5-2.0 keV image of the central region of ZW3146 shows the two inner edges at $3''$ and $8''$. (**b**) The right panel shows the edge at $35''$.

2.3 ZW3146 – Multiple Cold Fronts

ZW3146 is a moderately distant ($z = 0.2906$; 5.74 kpc per arcsec) cluster with a remarkably high mass deposition rate that was estimated to exceed 1000 $M_\odot$ yr^{-1} [13]. The Chandra image further demonstrates the remarkable nature of this cluster – on scales from $3''$ to $30''$ ($\sim$ 20 kpc to 170 kpc), three separate X-ray surface brightness edges are detected (see Fig. 3 and Forman et al. [22]). At the smallest radii, two edges are seen to the northwest and north of the center (see Fig.3a). The first, at a radius of $\sim 3''$ (17 kpc), spans an angle of nearly 180° with a surface brightness drop of almost a factor of 2. The second edge, at a radius of $\sim 8''$ (45 kpc) spans only 90° but has a surface brightness drop of almost a factor of 4. The third edge (see Fig. 3b) lies to the southeast,

about 35″ (200 kpc) from the cluster center, has a decrease of about a factor of 2, and, as with the first edge, extends over an angle of almost 180°.

The variety of morphologies and scales exhibited by these sharp edges or cold fronts is quite remarkable. Possibly the edges may arise from moving cold gas clouds that are the remnants of merger activity as observed in A2142 and A3667 or as oscillations (or "sloshing") of the cool gas at the center of the cluster potential as observed in A1795 [38]. The extremely regular morphology of ZW3146 on large linear scales seems to exclude a recent merger and, hence, "sloshing" of the gas seems the more likely explanation for the observed edges. High resolution, large scale structure simulations show that dense halos, formed at very early epochs, would not be disrupted as clusters collapse [24,25]. While most of the dark matter halos, having galaxy size masses, are associated with the sites of galaxy formation, the larger mass halos also may survive (without their gas) or may have fallen into the cluster only recently. Hence, we might expect to find a range of halo mass distributions moving within the cluster potential. We speculate that, as these halos move, the varying gravitational potential could accelerate the cool dense gas that has accumulated in the cluster core and could produce the "sloshing" needed to give rise to the multiple surface brightness edges observed in some clusters. Simulations are needed to confirm such a possibility.

2.4 CL0657 – A Prototypical Cluster Shock Front

CL0657 ($z = 0.296$) was discovered by Tucker et al. as part of a search for "failed" clusters, clusters that were X-ray bright but had few, if any, optical galaxies [47]. From ASCA observations, this cluster was found to have a remarkably hot gas temperature of about 17 keV, making it the hottest cluster known [48].

The Chandra image of CL0657 shows the classic properties of a supersonic merger (see Markevitch et al. for a detailed discussion of this cluster [39]). We see a dense (cold) core moving to the west after having traversed, and disrupted, the core of the main cluster. Leading the cold, dense core is a density discontinuity which appears as a shock front (Mach cone) and is confirmed by the spectral data to be hotter to the east (trailing the shock), unlike the cold fronts discussed above (or the eastern boundary of the bullet which also is a cold front). The detailed gas density parameters confirm that the "bullet" is moving to the west with a velocity of 3000–4000 km sec^{-1}, approximately 2-3 times the sound speed of the ambient gas. CL0657 is the first clear example of a relatively strong shock arising from cluster mergers.

The Chandra observation confirms the unusually high mean cluster temperature of 14-15 keV, but shows regions with temperatures as high as 20 keV. The unrelaxed nature of CL0657 urges caution in the use of high temperatures of a few extreme clusters to derive cosmological constraints. Since the present mean temperature is likely to differ from what it will become after the cluster achieves hydrostatic equilibrium, the derived cluster mass would be in error and would result in incorrect cosmological constraints.

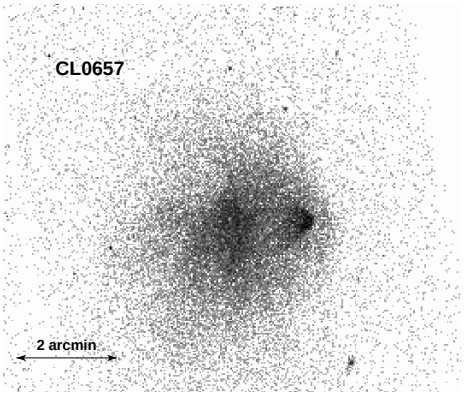

Fig. 4. The Chandra image of the cluster CL0657. The cluster exhibits the classic properties of a supersonic merger – a dense (cold) "bullet" traversing the hot cluster with a leading shock front (Mach cone). The gas parameters across the front imply the cold core is traversing the cluster at a supersonic velocity with a Mach number of $M \sim 2 - 3$. The disrupted core of the cluster can be seen to the east of the "bullet".

3 The Radio—X-ray Connection – or Bubbles, Bubbles Everywhere

Prior to the launch of Chandra, ROSAT observations of NGC1275 and M87 provided hints of complex interactions between radio emitting plasmas ejected from AGN within the nuclei of dominant, central cluster galaxies [2,3,8]. With the launch of Chandra, the interaction between the radio emitting plasma and the hot intracluster medium (ICM) has been observed in many systems and now can be studied in detail.

3.1 Hot Plasma Bubbles in Cluster and Galaxy Atmospheres

One of the first, and clearest, examples of the effect of plasma bubbles on the hot intracluster medium was found in the Perseus cluster around the bright active, central galaxy NGC1275 (3C84). First studied in ROSAT images[2], the radio emitting cavities to the north and south of NGC1275 are clearly seen in the Chandra images with bright X-ray emitting rims surrounding the cavities that coincide with the inner radio lobes [15]. For NGC1275/Perseus, the radio lobes are in approximate pressure equilibrium with the ambient, denser and cooler gas and the bright X-ray rims surrounding the cavities are softer than the ambient gas. The central galaxy in the Hydra A cluster also harbors X-ray cavities associated with radio lobes that also show no evidence for shock heating [42]. Both sets of radio bubbles, being of lower density than the ambient gas, must be buoyant.

The Chandra images of Perseus/NGC1275 also suggest the presence of older bubbles produced by earlier outbursts [15]. These older bubbles appear as X-ray surface brightness "holes", but unlike the inner bubbles, these outer holes

show no detectable radio emission, suggesting that the synchrotron emitting electrons may have decayed away leaving a heated, plasma bubble (see Fabian et al. who recently reported low frequency radio spurs extending towards the outer bubbles in NGC1275, consistent with this scenario [16]). Such bubbles, with no attendant radio emission, are seen by Chandra in the galaxy groups HCG62 and MKW3s [55,41].

The examples of bubbles described above concentrate on those around central dominant cluster galaxies. However, bubbles, and their effects are seen in more common early type galaxies. For example, in the E1 galaxy M84 (NGC4374), Chandra observed an unusual X-ray morphology which is explained by the effect of the radio lobes on the hot gas [17]. The X-ray emission appears $\mathcal{H}$-shaped, with a bar extending east-west with two nearly parallel filaments perpendicular to this bar. The complex X-ray surface brightness distribution arises from the presence of two radio lobes (approximately north and south of the galaxy) that produce two low density regions surrounded by higher density X-ray filaments. As with Perseus/NGC1275 and Hydra A, the filaments, defining the $\mathcal{H}$-shaped emission, have gas temperatures comparable to the gas in the central and outer regions of the galaxy and hence argue against any strong shock heating of the galaxy atmosphere by the radio plasma. By deriving the gas density surrounding the radio lobes, Finoguenov & Jones were able to calculate the strength of the magnetic field using the observed Faraday rotation. They inferred a line-of-sight magnetic field of 0.8μ Gauss [17].

3.2 Evolution of Buoyant Plasma Bubbles in Hot Gaseous Atmospheres

The 327 MHz high resolution, high dynamic range radio map of M87 shows a well-defined torus-like eastern bubble and a less well-defined western bubble, both of which are connected to the central emission by a column, and two very faint almost circular emission regions northeast and southwest of the center [43]. The correlation between X–ray and radio emitting features has been remarked by several authors [18,3,27].

Motivated by the similarity in appearance between M87 and hot bubbles rising in a gaseous atmosphere, Churazov et al. developed a simple model of the M87 bubbles which is generally applicable to the many bubble-like systems seen in the Chandra observations [9]. An initial buoyant, spherical bubble transforms into a torus as it rises through the galaxy or cluster atmosphere. By entraining cool gas as it rises, it exhibits a characteristic "mushroom" appearance, similar to an atmospheric nuclear explosion. This may qualitatively explain the correlation of the radio and X–ray emitting plasmas and naturally accounts for the thermal nature of the X-ray emission associated with the rising torus [3]. Finally, in the last evolutionary phase of an atmospheric explosion, the bubble reaches a height at which the ambient gas density equals that of the bubble. The bubble then expands to form a thin layer (a "pancake"). The large low surface brightness features in the M87 radio map could be just such pancakes – the final evolutionary phase of the bubbles. In the simulations performed by

Churazov et al. the buoyant bubbles behaved as expected and did produce the features observed in both X-rays and radio for M87. Although the exact form of the rising bubbles was sensitive to initial conditions, the toroidal structures were a common feature. Ambient gas was uplifted in the cluster atmosphere reducing the effects of gas cooling and flowing to the center and producing the "stem" of the mushroom that is brighter than the surrounding regions [9].

3.3 Explosive Cavities

NGC4636 is one of the nearest and most X-ray luminous "normal" elliptical galaxies (L_X $\sim$2$\times$10^{41} ergs s^{-1}). The first X-ray imaging observations of NGC4636 from Einstein showed that, like other luminous elliptical galaxies, NGC4636 was surrounded by an extensive hot gas corona [21].

The Chandra observation of NGC4636 shows a new phenomenon – shocks produced by nuclear outbursts (see Jones et al. for details of the Chandra observation of NGC4636 [33]). The high angular resolution Chandra image (see Fig. 5) shows symmetric, $\sim$ 8 kpc long, arm-like features in the X-ray halo surrounding NGC4636. The leading edges of these features are sharp and are accompanied by temperature increases of $\sim$ 30%, as expected from shocks propagating in a galaxy atmosphere.

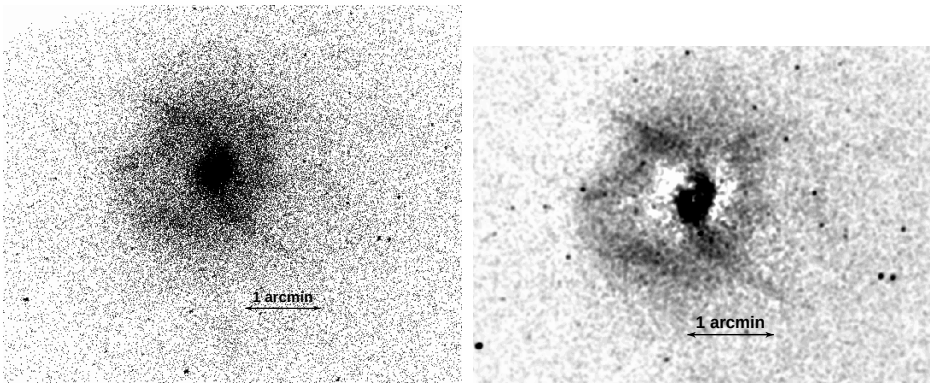

Fig. 5. (**a**) shows the 0.5-2.0 keV ACIS-S image of NGC4636 at full resolution (1 pixel = 0.492″). (**b**) shows the emission after an azimuthally symmetric model describing the galaxy corona has been subtracted. The remaining emission was smoothed with a two pixel Gaussian. Shocks from a nuclear outburst could produce the brighter arm-like structures, while the additional features could arise from other outbursts.

Although the sharpness of the edges of the NE and SW arms appears similar to the sharp edges found along "fronts" in clusters (see discussion and references above), the cluster "fronts" are cold, while those in NGC4636 are hot. Also, while the presence of sharp fronts suggests the possibility of an ongoing merger, the east-west symmetry of the halo structures, the similarity of this structure to

that seen around radio lobes, as well as the lack of a disturbed morphology in the stellar core or in the stellar velocities suggest an outburst from the nucleus as the underlying cause. In particular, the bright SW arm, the fainter NW arm and the bright NE arm can be produced by the projected edges of two paraboloidal shock fronts expanding about an east – west axis through the nucleus. A shock model is also consistent with the evacuated cavities to the east and west of the central region.

The size, symmetry, and gas density and temperature profiles of the shocks are consistent with a nuclear outburt of energy $\sim 6 \times 10^{56}$ ergs having occurred about $\sim 3 \times 10^6$ years ago. It is tempting to suggest that these outbursts are part of a cycle in which cooling gas fuels nuclear outbursts that periodically reheat the cooling gas. Such outbursts if sufficiently frequent could prevent the accumulation of significant amounts of cooled gas in the galaxy center.

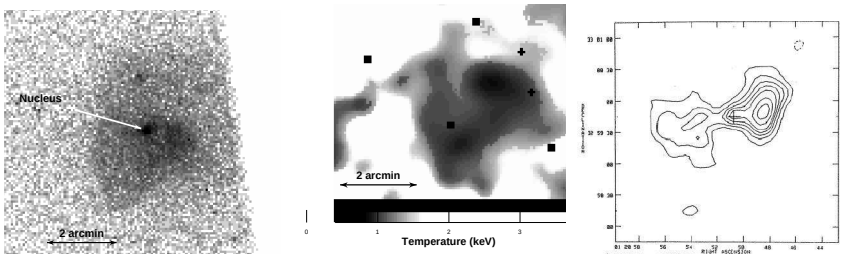

Fig. 6. (**a**) The 0.5-2.0 keV surface brightness distribution of NGC507. (**b**) The temperature map of the central region of NGC507. The galaxy center is cool as are the region to the west, the north-south edge to the east, and the edge to the south running from northwest to southeast. (**c**) The VLA radio map showing the central point source, a jet emanating to the west and two radio lobes [11]. The depression in the X-ray surface brightness to the west of the galaxy peak coincides with the western radio lobe.

3.4 NGC507 - the central galaxy in a group

NGC507 is the central galaxy in a nearby ($z = 0.016$) group that has been studied extensively in X-rays [34,40,6,23]. The galaxy is the site of a weak B2 radio source (luminosity $\sim 10^{37}$ ergs s^{-1}) [11]. The Chandra X-ray image, shown in Fig. 6a, covers only the central, high surface brightness emission of the group around NGC507. The 0.5-2.0 keV surface brightness distribution shows sharp edges to the southwest, southeast and north, reminiscent of those in the clusters A2142 and A3667. In addition to the edges, there are two X-ray peaks. The first, to the east, coincides with the nucleus of NGC507. A second peak, $1'$ to the west has no optical counterpart. However, comparing the X-ray and the radio map (Fig. 6a, c) shows that the western radio lobe lies precisely in the surface brightness trough between the nucleus and the peak to the west. Thus,

it seems likely that the radio lobe, probably a buoyant bubble, has displaced X-ray emitting gas generating a trough in the X-ray surface brightness distribution.

The origin of the peculiar sharp surface brightness discontinuities around NGC507 is unclear. The bright emission is well fit by a thermal model with gas temperatures near 1 keV, consistent with the mean ASCA temperature of 1.10 ± 0.05 keV [40]. The emission from the central region is resolved and hence the contribution from a central AGN is relatively small (see Forman et al. [22] for additional discussion of NGC507). Perhaps the X-ray surface brightness features arise from motion of NGC507 and its dark halo within the larger group potential as suggested for the multiple edges in clusters [38].

4 Conclusions

We did not expect the rich variety of new structures seen in the Chandra high angular resolution observations of clusters and early type galaxies. Instead of confirming our prejudices, Chandra has brought us a wealth of new information on the interaction of radio sources with the hot gas in both galaxy and cluster atmospheres. We see "edges" in many systems with hot and cold gas in close proximity and have been able to extract important new parameters of the ICM from their study. We have only barely begun to digest the import of the Chandra cluster and galaxy observations. We can only expect the unexpected as Chandra observations continue and as our understanding of how best to use this new observatory matures.

We acknowledge support from NASA contract NAS8 39073, NASA grants NAG5-3065 and NAG5-6749 and the Smithsonian Institution.

References

1. H. Bohringer, U. Briel, R. Schwarz, W. Voges, G. Hartner, J. Trumper: Nature **368**, 828 (1994)
2. H. Bohringer et al.: MNRAS **264**, L25 (1993)
3. H. Bohringer, P. Nulsen, R. Braun, A. Fabian: MNRAS **274**, L67 (1995)
4. U. Briel et al.: A&A, **246**, L10 (1991)
5. U. Briel & J. Henry: A&A, **259**, L31 (1992)
6. D. Buote & A. Fabian: MNRAS, **296**, 977 (1998)
7. E. Churazov, et al.: ApJ, **520**, 105 (1999)
8. E. Churazov, W. Forman, C. Jones, H. Bohringer: A&A, **356**, 788 (2000a)
9. E. Churazov et al.: ApJ **554**, 261 (2001)
10. R. Donnelly et al.: ApJ **500**, 138 (1998)
11. H. R. de Ruiter, P. Parma, P., C. Fanti, R. Fanti: A&AS, **65**, 111 (1986)
12. F. Durret, F. et al.: A&A, **335**, 41 (1998)
13. A. Edge et al.: MNRAS, **270**, L1 (1994)
14. A. Fabian, J. Schwarz, W. Forman: MNRAS **192**, 135 (1980)
15. A. Fabian et al.: MNRAS **318**, L65 (2000)
16. A. C. Fabian, A. Celotti, K.M. Blundell, N.E. Kassim, R.A. Perley: MNRAS in press, astro-ph/0111418 (2001)

17. A. Finoguenov, C. Jones: ApJL **547**, L107 (2001)
18. E. Feigelson, P. Wood, E. Schreier, D. Harris, M. Reid: ApJ **312**, 101 (1987)
19. W. Forman, J. Bechtold, W. Blair, R. Giacconi, L. van Speybroeck, C. Jones: ApJL **243**, 133 (1981)
20. W. Forman, J. Schwarz, C. Jones, W. Liller, A. Fabian: ApJL **234**, 27 (1979)
21. W. Forman, C. Jones, W. Tucker: ApJ **293**, 102 (1985)
22. W. Forman, M. Markevitch, C. Jones, A. Vikhlinin, E. Churazov, astro-ph/0110087 (2001)
23. Y. Fukazawa: PASJ, **50**, 187 (1998)
24. S. Ghigna, B. Moore, F. Governato, G. Lake, T. Guinn, J. Stadel: MNRAS, **300**, 146 (1998)
25. S. Ghigna, B. Moore, F. Governato, G. Lake, T. Guinn, J. Stadel: ApJ, **544**, 616 (2000)
26. J. Gunn, & R. Gott: ApJ **176**, 1 (1972)
27. D. Harris, F. N. Owen, J. A. Biretta, W. Junor: Diffuse Thermal and Relativistic Plasma in Galaxy Clusters eds. H.Böhringer, L.Feretti, P. Schuecker, MPE Report **271**, 111 (1999)
28. M. Henriksen & M. Markevitch: ApJ **466**, L79 (1996)
29. J. P. Henry & U. Briel: ApJL **443**, 9 (1995)
30. H. Honda et al.: ApJL **473**, 71 (1996)
31. C. Jones et al.: ApJL **234**, 21 (1979)
32. C. Jones & W. Forman: ApJ **276**, 38 (1984)
33. C. Jones, W. Forman, A. Vikhlinin, M. Markevitch, L. David, A. Warmflash, S. Murray, P. E. J. Nulsen: submitted to **ApJL**, astro-ph/0108114 (2001)
34. D. Kim & G. Fabbiano: ApJ **441**, 182 (1995)
35. K. Makishima et al.: PASJ, **53**, 401 (2001)
36. M. Markevitch et al.: ApJ **541**, 542 (2000)
37. M. Markevitch, C. Sarazin, A. Vikhlinin: ApJ **521**, 526 (1999)
38. M. Markevitch, A. Vikhlinin, P. Mazzotta: ApJL **562**, L153 (2001)
39. M. Markevitch et al.: ApJL in press, astro-ph/0110468 (2001)
40. H. Matsumoto et al.: ApJ **482**, 133 (1997)
41. P. Mazzotta et al.: ApJL in press, astro-ph/0107557 (2001)
42. B. McNamara et al.: ApJL **534**, 135 (2000)
43. F. Owen, J. Eilek, N. Kassim: ApJ **543**, 611 (2000)
44. T. Ponman et al.: Nature, **369**, 462 (1994)
45. F. Rangarajan, D. White, H. Ebeling, A. Fabian: MNRAS, **277**, 1047 (1995)
46. S. Schindler, B. Binggeli, H. Bohringer: A&A **343**, 420 (1999)
47. W. Tucker, H. Tananbaum, & R. Remillard: ApJ **444**, 532 (1995)
48. W. Tucker et al.: ApJ **496**, L5 (1998)
49. M. Van Haarlem & R. Van de Weygaert: ApJ **418**, 544 (1993)
50. A. Vikhlinin et al.: ApJL **520**, 1 (1999)
51. A. Vikhlinin, W. Forman, C. Jones: ApJ **435**, 162 (1994)
52. A. Vikhlinin, W. Forman, C. Jones: ApJL **474**, 7 (1997)
53. A. Vikhlinin, M. Markevitch, S. Murray: ApJ **551** 160 (2000a)
54. A. Vikhlinin, M. Markevitch, S. Murray: ApJ **549**, L47 (2000b)
55. J. Vrtilek et al. , in preparation and IAP 2000 Workshop (2001)
56. D. White, A. Fabian, W. Forman, C. Jones, C. Stern: ApJ **375**, 35 (1991)